DOI: 10.13009/EUCASS2019-420

Secondary resonances due to the solar radiation pressure in the vicinity of the global navigation satellites regions

Eduard Kuznetsov, Vladislav Gusev and Ivan Malyutin
Ural Federal University
Lenina Avenue, 51, Yekaterinburg, Russia 620000, eduard.kuznetsov@urfu.ru

Abstract

The secondary resonances due to solar radiation pressure are investigated in the vicinity of orbits of the global navigation systems GLONASS (main resonance is 8:17), GPS (main resonance is 1:2), BeiDou (main resonance is 7:13), and Galileo (main resonance is 10:17). The secondary resonances were considered for both the main resonances and the sub-resonances *i*- and *e*-types. The secondary resonances locations were estimated analytically and were improved by numerically. The secondary resonance zones were found for both low (0.02, 0.2, and 1 m^2/kg) and high (10 m^2/kg and more) area-to-mass ratios. The secondary resonances have a significant effect on the dynamical evolution of objects with area-to-mass ratio 10 m^2/kg and more. This result is very important when describing the long-term orbital evolution of space debris.

1. Introduction

Valk et al. [1] found a relevant class of secondary resonances on both sides of the well-known pendulum-like pattern of geostationary objects. They have considered the secondary resonances due to solar radiation pressure with a resonant argument $\Psi = k\Phi \pm \lambda_\odot$. Here Φ is a resonant argument of a main resonance 1:1 and $\lambda_\odot$ is the ecliptic longitude of the Sun. The secondary resonances were detected for objects with high area-to-mass ratio γ = 10 m^2/kg and more. Detailed investigation of the secondary resonances near the geosynchronous orbits performed in [2].
In the present work, the secondary resonances near GLONASS, GPS, BeiDou, and Galileo orbits are investigated both analytical and numerical methods.

2. Methods

We consider motion in the vicinity of GLONASS, GPS, BeiDou, and Galileo regions which situated near 8:17, 1:2, 7:13, and 10:17 resonance zones respectively. We take sub-resonances *i*- and *e*-types into account to detailed investigate dynamical evolution of space debris in this region. Let's are three resonant arguments [3, 4]

$$\begin{aligned} \Phi_1 &= p\,(M + \Omega + g) \;-\; q\,S = \nu_1 t, \\ \Phi_2 &= p\,(M + g) + q\,(\Omega \;-\; S) = \nu_2 t, \\ \Phi_3 &= p\,M + q\,(\Omega + \mathrm{g} \;-\; S) = \nu_3 t \end{aligned} \qquad \textbf{(1)}$$

with frequencies

$$\begin{aligned} \nu_1 &= p\left(n_M + n_\Omega + n_g\right) \;-\; q\,\omega_\oplus, \\ \nu_2 &= p\left(n_M + n_g\right) \;-\; q\,(n_\Omega \;-\; \omega_\oplus), \\ \nu_3 &= p\,n_M \;-\; q\left(n_\Omega + n_g \;-\; \omega_\oplus\right). \end{aligned} \qquad \textbf{(2)}$$

Here Φ_1, Φ_2, and Φ_3 are the resonant arguments of the main resonance and two sub-resonances of *i*- and *e*-types, correspondently.
The condition $\nu_1 \approx 0$ corresponds to the resonance between the mean motion of the satellite and the Earth's angular velocity $\omega_\oplus$. The condition $\nu_2 \approx 0$ corresponds to an *i*-type resonance, under which the position of the ascending node

DOI: 10.13009/EUCASS2019-420

of the orbit repeats periodically in a rotating coordinate system. The condition $\nu_3 \approx 0$ corresponds to a *e*-type resonance at which the position of the line of apsides is considered.
We will study sets of resonant multiplets which consist of secondary resonance and two secondary sub-resonances of *i*- and *e*-types due to the solar radiation pressure with the resonant arguments

$$\Psi_{ks\pm} = k\,\Phi_s \pm \lambda_\odot. \quad \textbf{(3)}$$

and frequencies

$$\mathrm{f}_{ks\pm} = k\,\nu_s \pm n_\odot. \quad \textbf{(4)}$$

The conditions $f_{ks\pm} \approx 0$ give the resonant values of the semi-major axes (see Table 1) which correspond to the secondary resonances due to the solar radiation pressure.

Table 1: Resonant values of the semi-major axis for main secondary resonances $\Psi_{k1\pm}$

Resonant argument	***a* [km]**			
	GLONASS	**GPS**	**BeiDou**	**Galileo**
Ψ_{11-}	25 506.9	26 537.7	27 903.1	29 598.2
Ψ_{21-}	25 508.3	26 549.7	27 905.1	29 599.8
Ψ_{31-}	25 508.8	26 553.7	27 905.8	29 600.3
Φ_1	25 509	26 559	27 906	29 600.3
Ψ_{31+}	25 510.6	26 569.9	27 908.4	29 602.4
Ψ_{21+}	25 511.0	26 573.9	27 909.0	29 602.9
Ψ_{11+}	25 512.4	26 586.0	27 911.0	29 604.5

3. Numerical simulation

The resonant values of the semi-major axis have improved from a numerical simulation. Orbital evolution of objects is modelled with the help of "Numerical Model of Motion of Artificial Satellites" [5, 6] developed at the Tomsk State University. The model of perturbing forces takes into account the major perturbing factors: the gravitational field of the Earth (EGM96 model [7], harmonics up to the 27th order and degree, inclusive), the gravitation of the Moon and the Sun, the tides of the Earth, the direct radiation pressure taking into consideration the shadow of the Earth (coefficient of reflection of the satellite surface K = 1.44), the Poynting–Robertson effect, and the atmospheric drag. The equations of motion are integrated by the Everhart's method of the 19th order.

Initial data correspond to a nearly circular orbit with the eccentricity e = 0.001. Initial inclination depends on the navigation system. Initial values of longitude of ascending node Ω are equal to 0°, 90°, 180°, and 270°. The argument of pericenter g = 0.45804°. In this case, the pericenter is directed toward the Sun when Ω = 0°. Area-to-mass ratio γ is varied from low values corresponding to satellites γ = 0.02 and 0.2 m^2/kg to high values γ = 1, 10, 20 m^2/kg and more which correspond to space debris. Dynamical evolution covers a time spans of 24 or 240 years. Initial epoch T_0 is $00^h\ 00^m\ 00^s$ UTC 21.03.1958.

4. Results

4.1 Multiplets of secondary resonances near the GLONASS region

The results of numerical simulation show that the semi-major axis has secular perturbations due to the Poynting–Robertson effect and an object pass through the secondary resonance zones. The resonant argument $\Psi_{ks\pm}$ librates when the object is situated in the resonance zone. The secondary resonance zones were found for low (γ = 0.02 and 0.2 m^2/kg), moderate (γ = 1 m^2/kg) and high (γ = 10 m^2/kg and more) area-to-mass ratios.
Table 2 gives improved estimations of the resonant values of the semi-major axis from results of numerical simulation. Dashes in cells correspond to values which were not determinate from the numerical simulation data. Zones of the secondary resonances and sub-resonances are tightly situated concerning the main resonance and sub-resonances.
As shown in Fig. 1 and 2, the secondary resonances and sub-resonances are overlapped. Resonance overlapping may lead to stochastic orbital evolution. However secondary resonances do not a significant influence on the evolution of positional elements in the vicinity of GLONASS region (see Fig. 3).

DOI: 10.13009/EUCASS2019-420

Table 2: Resonant values of the semi-major axis for secondary resonances in the GLONASS region from a numerical simulation

Ψ	*a* [km]	Ψ	*a* [km]	Ψ	*a* [km]
Ψ_{11-}	25 506.1	Ψ_{12-}	25 505.1	Ψ_{13-}	—
Ψ_{21-}	25 507.2	Ψ_{22-}	25 507.2	Ψ_{23-}	—
Ψ_{31-}	25 507.3	Ψ_{32-}	—	Ψ_{33-}	—
Φ_1	25 508	Φ_2	25 508	Φ_3	—
Ψ_{31+}	25 509.3	Ψ_{32+}	—	Ψ_{33+}	—
Ψ_{21+}	25 510.1	Ψ_{22+}	25 509.1	Ψ_{23+}	—
Ψ_{11+}	25 511.2	Ψ_{12+}	25 510.2	Ψ_{13+}	—

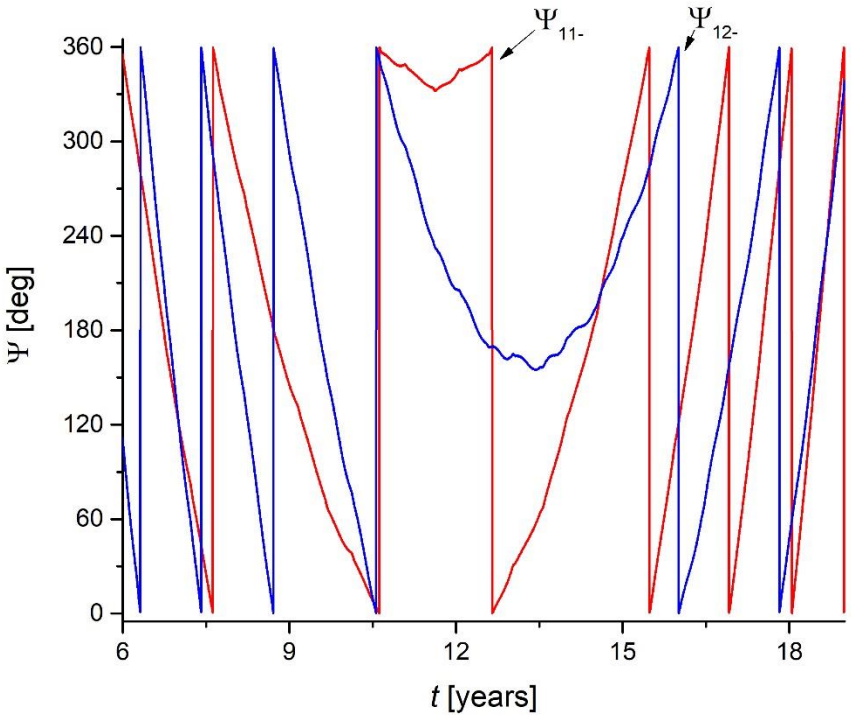

Figure 1: Evolution of resonant arguments Ψ_{11-} and Ψ_{12-} for area-to-mass ratio $\gamma = 10$ m^2/kg

4.2 Multiplets of secondary resonances near the GPS region

The numerical simulation data show that the semi-major axis has secular perturbations due to the Poynting–Robertson effect and an object pass through the secondary resonance zones. The secondary resonance zones were found for all considered values of the area-to-mass ratios.

Table 3 gives improved estimations of the resonant values of the semi-major axis from the numerical simulation data for the secondary resonance and sub-resonances. The secondary resonances and sub-resonances are well separated contrary to the GLONASS region.

Figures 4-6 show that the secondary resonances and sub-resonances are overlapped but the area-to-mass ratio is low ($\gamma = 0.2$ m^2/kg). The magnitude of oscillation of the semi-major axis is changed when the object is passing through the secondary resonances and sub-resonances. Secondary resonances overlapping also leads to a variation of the semi-major axis magnitude oscillations. Correlation between libration of resonant argument and variation of the magnitude of oscillation of the semi-major axis is clear for a moderate value of the area-to-mass ratio (as shown in Fig. 7).

Passing through secondary resonance for the objects with the high area-to-mass ratio ($\gamma = 10$ m^2/kg and more) produces qualitative changes in the evolution of the semi-major axis (see Fig. 8 and 9). In the secondary resonance (t = 0–12 years in Fig. 8 and t = 11–17 years in Fig. 9) the semi-major axis decreases. After that mean value of the semi-major axis is a near constant.

DOI: 10.13009/EUCASS2019-420

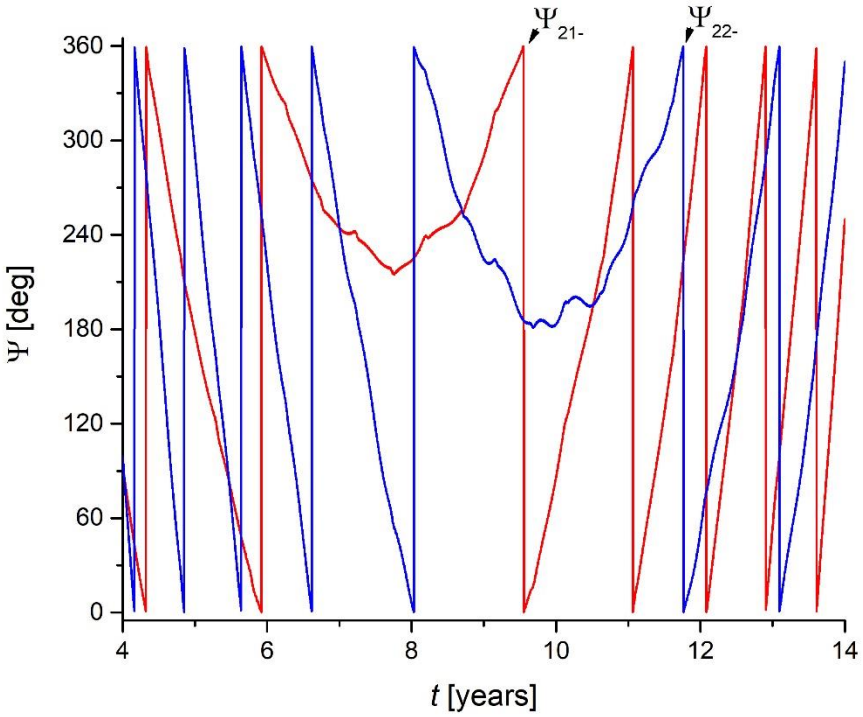

Figure 2: Evolution of resonant arguments Ψ_{21-} and Ψ_{22-} for area-to-mass ratio $\gamma = 10$ m^2/kg

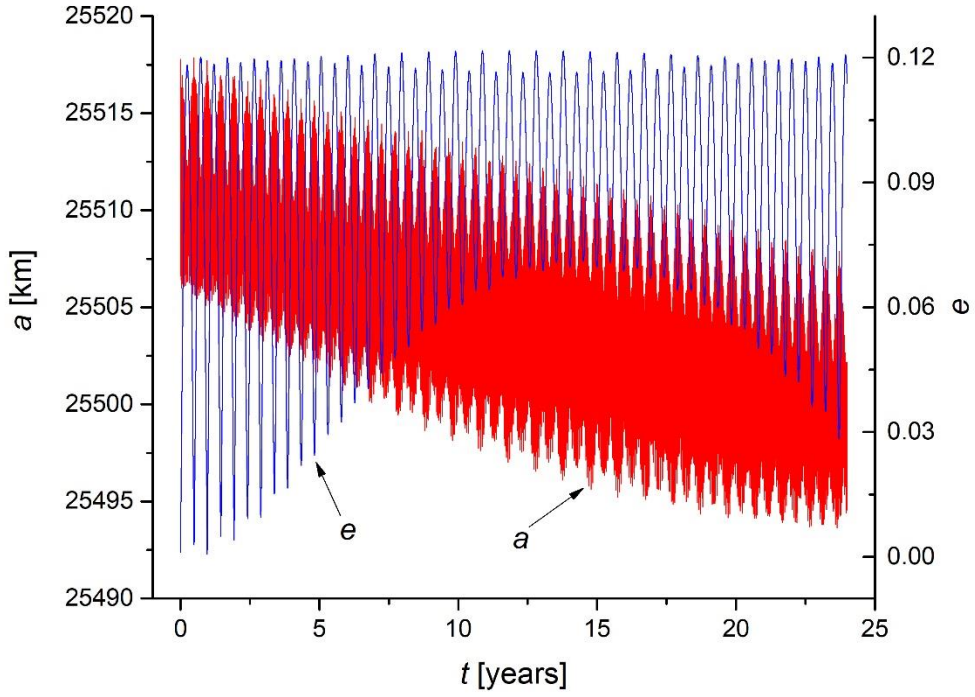

Figure 3 : Evolution of semi-major axis *a* (red) and eccentricity *e* (blue) for area-to-mass ratio $\gamma = 10$ m^2/kg

The secondary *i*-type sub-resonances have an insufficient effect on the evolution of the inclination (see Fig. 10 and 11) as well as the secondary *e*-type sub-resonances effect on the evolution of the eccentricity.

DOI: 10.13009/EUCASS2019-420

Table 3. Resonant values of the semi-major axis for secondary resonances in the GPS region from a numerical simulation

Ψ	**a [km]**	**Ψ**	**a [km]**	**Ψ**	**a [km]**
Ψ_{11-}	26 537.4	Ψ_{12-}	26 536.4	Ψ_{13-}	26 536.4
Ψ_{21-}	26 549.0	Ψ_{22-}	26 548.1	Ψ_{23-}	26 549.0
Ψ_{31-}	26 553.6	Ψ_{32-}	26 552.7	Ψ_{33-}	26 552.7
Φ_1	26 559	Φ_2	26 558	Φ_3	26 558
Ψ_{31+}	26 569	Ψ_{32+}	26 568	Ψ_{33+}	26 568
Ψ_{21+}	26 573.4	Ψ_{22+}	26 572.5	Ψ_{23+}	26 573.4
Ψ_{11+}	26 585.3	Ψ_{12+}	26 584.6	Ψ_{13+}	26 585.1

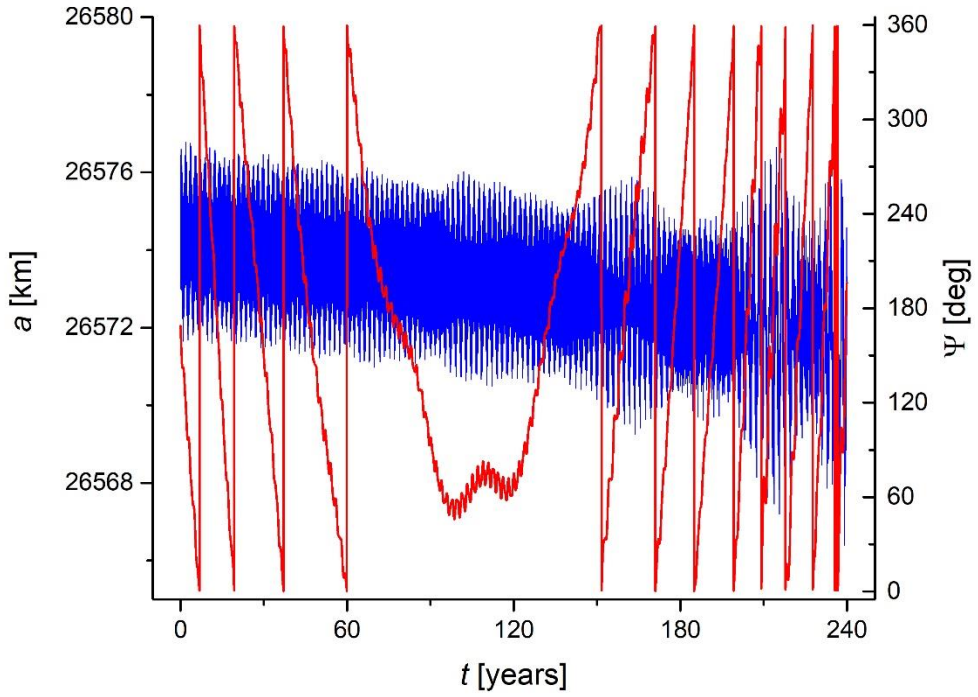

Figure 4: Evolution of semi-major axis *a* (blue) and resonant argument Ψ_{21+} (red) for area-to-mass ratio γ = 0.2 m²/kg

4.3 Multiplets of secondary resonances near the BeiDou region

The results of numerical simulation show that the semi-major axis has secular perturbations due to the Poynting–Robertson effect and an object pass through the secondary resonance zones. The resonant argument $\Psi_{ks\pm}$ librates when the object is situated in the resonance zone. The secondary resonance zones were found for low (γ = 0.02 and 0.2 m²/kg), moderate (γ = 1 m²/kg) and high (γ = 10 m²/kg and more) area-to-mass ratios.
Table 4 gives improved estimations of the resonant values of the semi-major axis from results of numerical simulation. Dashes in cells correspond to values which were not determinate from the numerical simulation data. Zones of the secondary resonances and sub-resonances are tightly situated concerning the main resonance and sub-resonances.

DOI: 10.13009/EUCASS2019-420

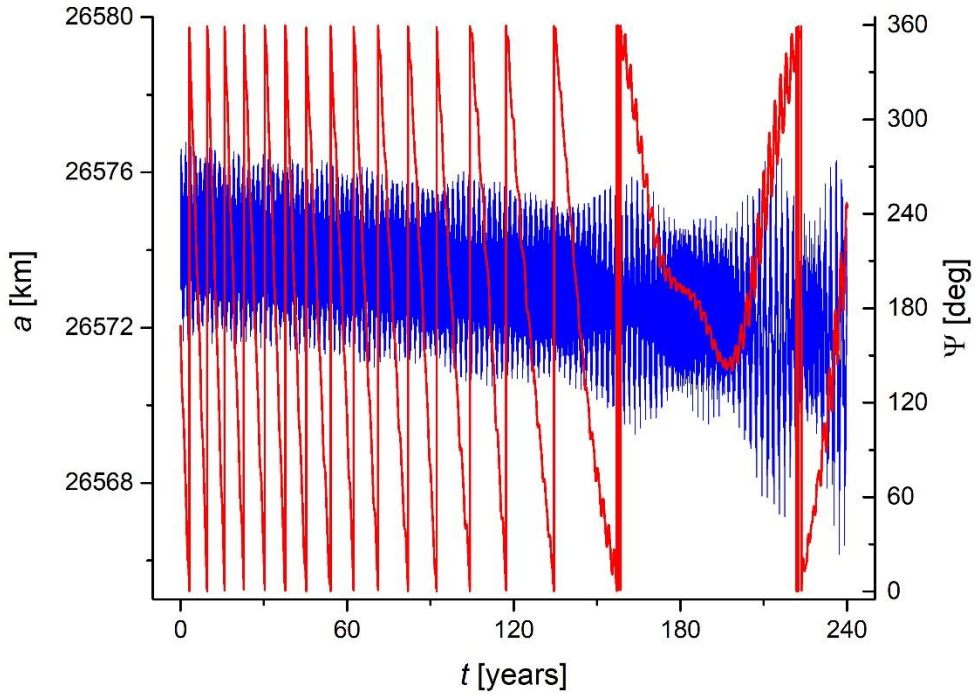

Figure 5: Evolution of semi-major axis *a* (blue) and resonant argument Ψ_{22+} (red) for area-to-mass ratio γ = 0.2 m^2/kg

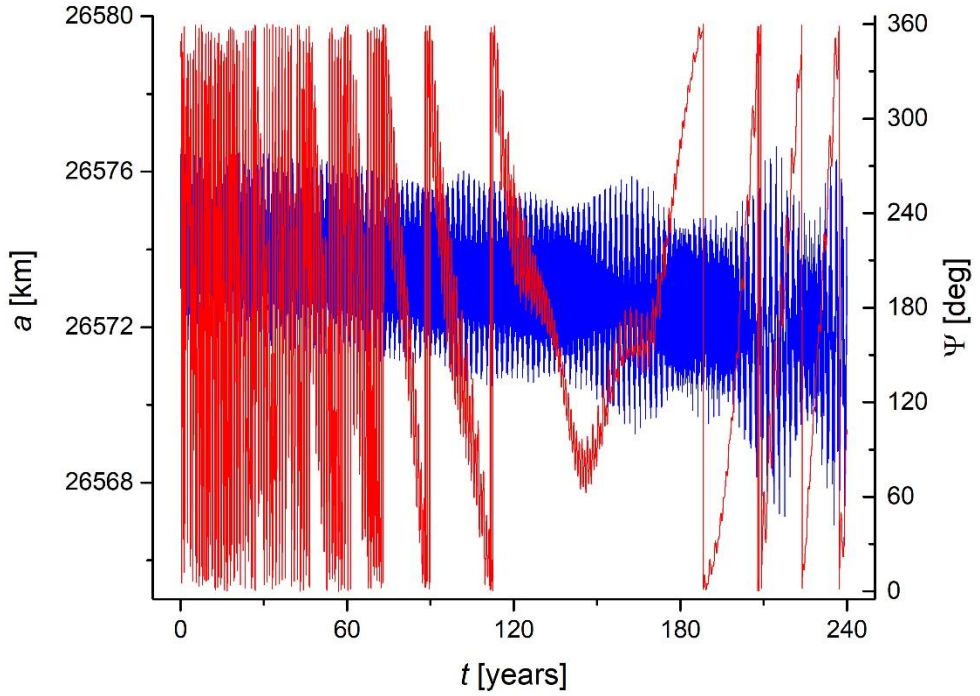

Figure 6: Evolution of semi-major axis *a* (blue) and resonant argument Ψ_{23+} (red) for area-to-mass ratio γ = 0.2 m^2/kg

DOI: 10.13009/EUCASS2019-420

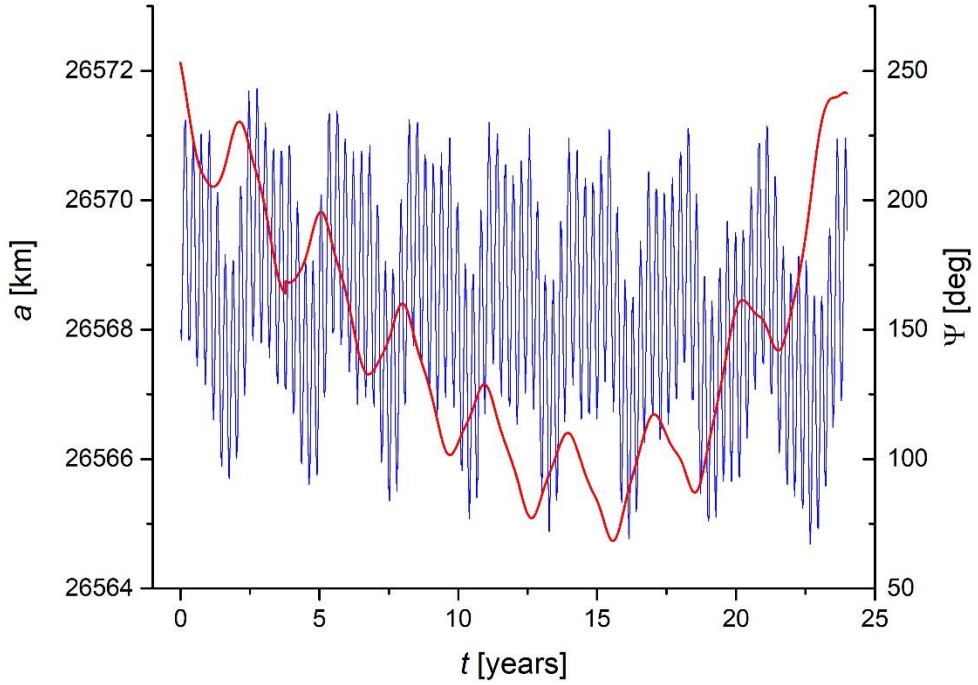

Figure 7: Evolution of semi-major axis *a* (blue) and resonant argument Ψ_{32+} (red) for area-to-mass ratio γ = 1 m^2/kg

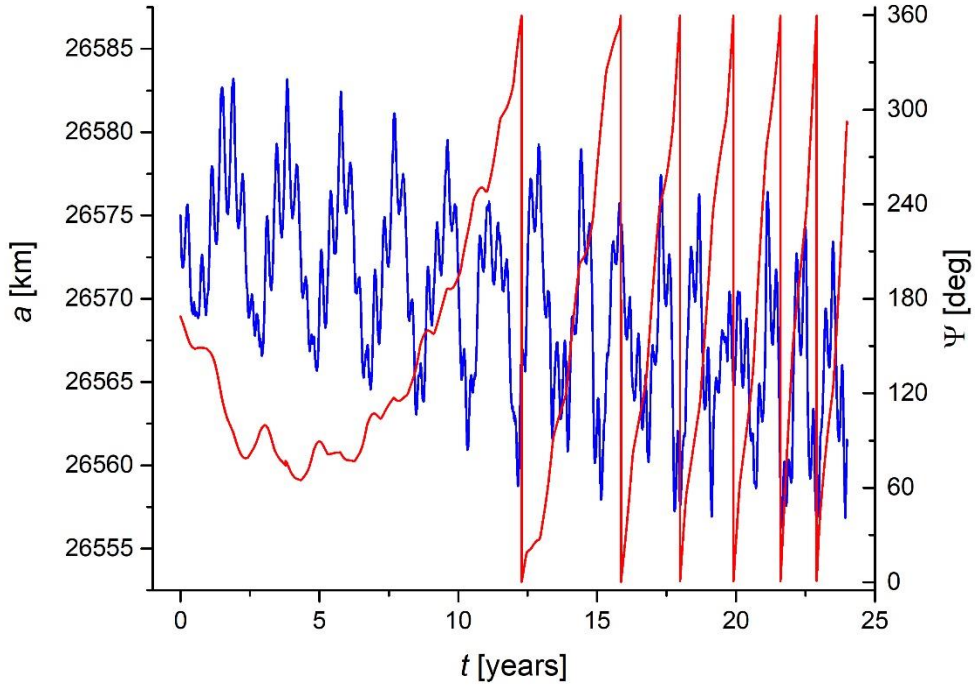

Figure 8: Evolution of semi-major axis *a* (blue) and resonant argument Ψ_{21+} (red) for area-to-mass ratio γ = 10 m^2/kg

DOI: 10.13009/EUCASS2019-420

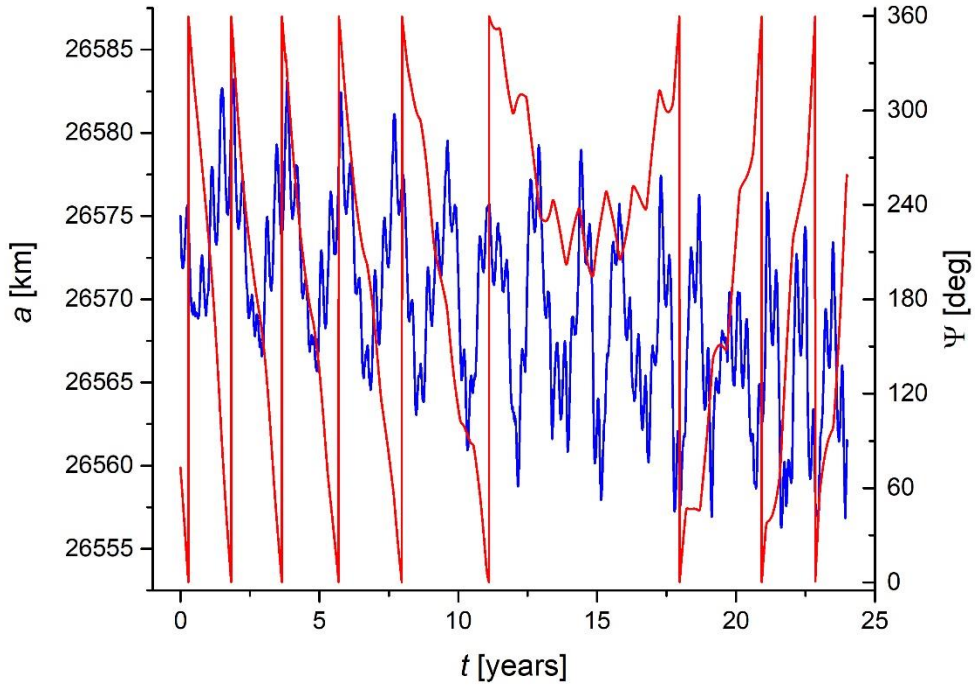

Figure 9: Evolution of semi-major axis *a* (blue) and resonant argument Ψ_{31+} (red) for area-to-mass ratio γ = 10 m^2/kg

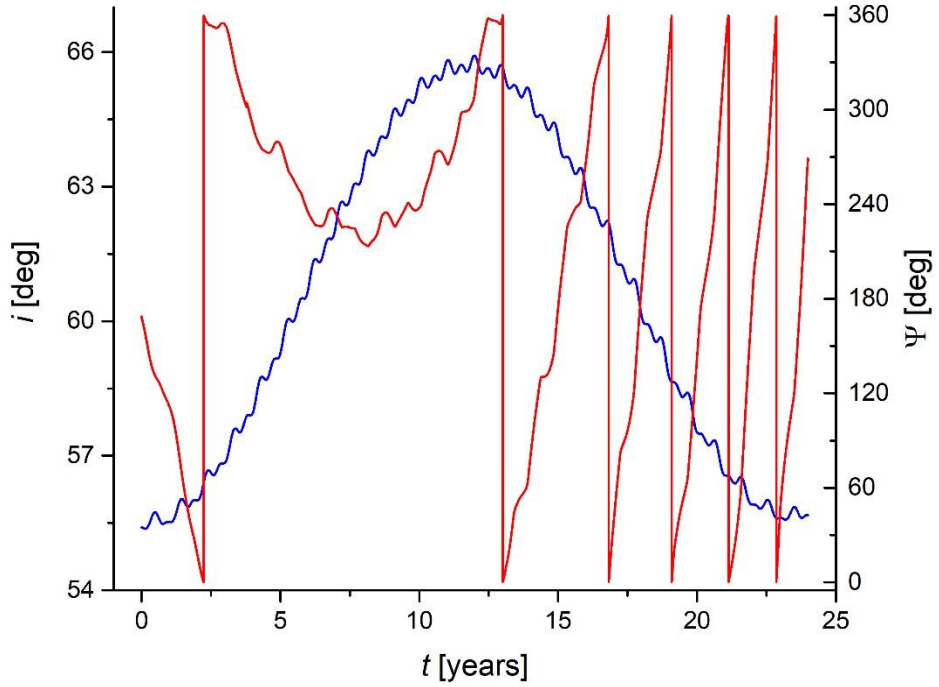

Figure 10: Evolution of inclination *i* (blue) and resonant argument Ψ_{22+} (red) for area-to-mass ratio γ = 10 m^2/kg

DOI: 10.13009/EUCASS2019-420

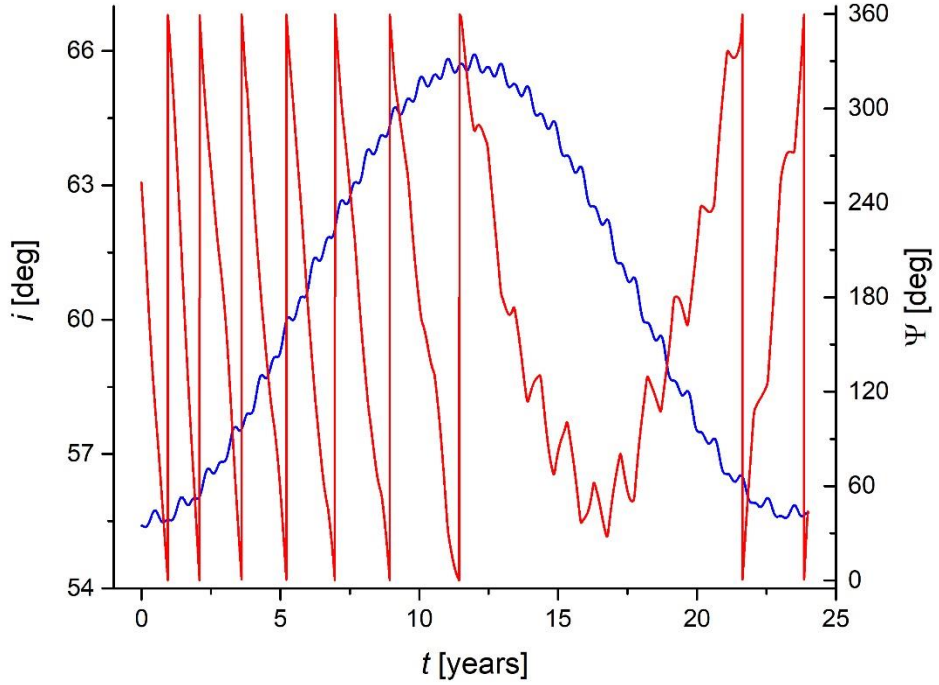

Figure 11: Evolution of inclination i (blue) and resonant argument Ψ_{32+} (red) for area-to-mass ratio γ = 10 m^2/kg

Table 4. Resonant values of the semi-major axis for secondary resonances in the BeiDou region from a numerical simulation

Ψ	a [km]	Ψ	a [km]	Ψ	a [km]
Ψ_{11-}	—	Ψ_{12-}	—	Ψ_{13-}	27 902.0
Ψ_{21-}	27 904.8	Ψ_{22-}	27 903.5	Ψ_{23-}	27 903.8
Ψ_{31-}	27 905.0	Ψ_{32-}	27 904.5	Ψ_{33-}	27 904.7
Φ_1	27 906	Φ_2	27 905.5	Φ_3	27 905.5
Ψ_{31+}	27 907.7	Ψ_{32+}	27 907.4	Ψ_{33+}	27 907.4
Ψ_{21+}	27 908.4	Ψ_{22+}	27 907.6	Ψ_{23+}	27 907.6
Ψ_{11+}	27 901.8	Ψ_{12+}	27 909.6	Ψ_{13+}	27 909.6

4.4 Multiplets of secondary resonances near the Galileo region

The results of numerical simulation show that the semi-major axis has secular perturbations due to the Poynting–Robertson effect and an object pass through the secondary resonance zones. The resonant argument $\Psi_{ks\pm}$ librates when the object is situated in the resonance zone. The secondary resonance zones were found for low (γ = 0.02 and 0.2 m^2/kg), moderate (γ = 1 m^2/kg) and high (γ = 10 m^2/kg and more) area-to-mass ratios.
Table 5 gives improved estimations of the resonant values of the semi-major axis from results of numerical simulation. Dashes in cells correspond to values which were not determinate from the numerical simulation data. Zones of the secondary resonances and sub-resonances are tightly situated concerning the main resonance and sub-resonances.

DOI: 10.13009/EUCASS2019-420

Table 5. Resonant values of the semi-major axis for secondary resonances in the Galileo region from a numerical simulation

Ψ	**a [km]**	**Ψ**	**a [km]**	**Ψ**	**a [km]**
Ψ_{11-}	29 598.3	Ψ_{12-}	29 597.5	Ψ_{13-}	29 598.0
Ψ_{21-}	29 599.5	Ψ_{22-}	29 598.7	Ψ_{23-}	29 598.5
Ψ_{31-}	29 600.3	Ψ_{32-}	29 599.5	Ψ_{33-}	29 599.0
Φ_1	29 601	Φ_2	29 600	Φ_3	29 600
Ψ_{31+}	29 602.4	Ψ_{32+}	29 601.9	Ψ_{33+}	29 602.4
Ψ_{21+}	29 602.5	Ψ_{22+}	29 602.4	Ψ_{23+}	29 603.4
Ψ_{11+}	29 601.9	Ψ_{12+}	29 603.5	Ψ_{13+}	29 604.3

5. Discussion

There is the secondary resonance overlapping for the high area-to-mass ratio values in the GLONASS region and all considered area-to-mas ratio values in the GPS, BeiDou, and Galileo regions. Secondary resonances do not significantly influence on the evolution of positional elements in the vicinity of GLONASS, BeiDou, and Galileo regions in spite of a resonance overlapping. Secondary resonances make a significant influence on the evolution of positional elements in the vicinity of GPS region.

The secondary resonances regions do not advantage for choose of disposal orbits. Both the low area-to-mass ratio objects (e.g., satellites) and the high area-to-mass ratio objects (e.g., space debris) pass through the secondary resonances under the Poynting–Robertson effect.

6. Conclusions

The secondary resonances and sub-resonances due to solar radiation pressure have found in the vicinity of the GLONASS, GPS, BeiDou, and Galileo regions. The secondary resonances are necessary to take into account the design of disposal orbits but that resonances may make a significant influence on the orbital evolution of space debris. Secondary resonance overlapping may produce stochastic orbital evolution on long time intervals. We are planning to study that effect in the future.

Acknowledgements. This work was supported by the Ministry of Education and Science of the Russian Federation (the basic part of the State assignment, RK no. AAAA-A17-117030310283-7) and the Government of the Russian Federation (Act 211, contract no. 02.A03.21.0006).

References

[1] Valk, S., Delsate, N., Lemaître, A., and T. Carletti. 2009. Global dynamics of high area-to-mass ratios GEO space debris by means of the MEGNO indicator. *Adv. Space Res.* 43:1509–1526.

[2] Lemaître, A., Delsate, N., and S. Valk. 2009. A web of secondary resonances for large *A/m* geostationary debris. *Celest. Mech. Dyn. Astr.* 104:383–402.

[3] Allan, R.R. 1967. Resonance effects due to the longitude dependence of the gravitational field of a rotating primary. *Planet. and Sp. Sci.* 15:53–76.

[4] Allan, R.R. 1967. Satellites resonance with the longitude-dependent gravity. II. Effects involving the eccentricity. *Planet. and Sp. Sci.* 15:1829–1845.

[5] Bordovitsyna, T.V., Baturin, A.P., Avdyushev, V.A., and P.V. Kulikova. 2007. Numerical model for simulating numerically an artificial Earth satellite motion. New version. *Izv. Vyssh. Uchebn. Zaved. Fiz.* 12/2:60–65 (in Russian).

[6] Bordovitsyna, T.V., Tomilova, I.V., and I.N. Chuvashov. 2012. The effect of secular resonances on the long-term orbital evolution of uncontrollable objects on satellite radio navigation systems in the MEO region. *Solar System Research*. 46:329–340.

[7] Lemoine, F.G., Kenyon, S.C., Factor, J.K., Trimmer, R.G., Pavlis, N.K., Chinn, D.S., Cox, C.M., Klosko, S.M., Luthcke, S.B., Torrence, M.H., Wang, Y.M., Williamson, R.G., Pavlis, E.C., Rapp, R.H., and T.R. Olson. 1998. The development of the joint NASA GSFC and National Imagery and Mapping Agency (NIMA) geopotential model EGM96. NASA/TP-1998-206861. GSFC.